# THERMAL PROPERTIES OF CRYSTALS AND POLYMERS AT STATIC HIGH PRESSURES

J. R. Carney,[+] H. D. Ladouceur,* T. P. Russell,[+] and G. I. Pangilinan[+]

[+]Dynamics and Diagnostics Division
Research and Technology Department
Naval Surface Warfare Center – Indian Head
Indian Head, MD 20640

*Chemistry Division, Code 6111
Naval Research Laboratory
Washington DC 20375

The thermal properties of materials at static high pressure were determined by dynamic spectroscopic methods. Laser-induced ruby fluorescence lines were used to monitor the progression of a thermal wave through a selected solid material encased in a diamond anvil cell. The temporal profile and magnitude of this wave were used to determine thermal properties of materials at high pressures and a pressure-dependent set of data ensued. Analytical and numerical simulations were used to analyze experimental results, yielding values for k (thermal conductivity), $\alpha$ (thermal diffusivity), and $C_p$ (heat capacity) at high pressures. The derivations and assumptions of these simulations will be discussed. Results will be discussed for NaCl and the polymeric binder, Teflon.

## INTRODUCTION

The inherent difficulty in measuring physical and chemical properties of materials at elevated pressures limits our understanding of shock and detonation processes. Current technologies using electrical and optical gauges allow measurements of mechanical properties such as shock arrival time, shock speed, and peak pressures. However, ensuing processes such as deformations, heat transfer, and chemical reactions are still unknown. Theories and models, together with experimental measurements, are needed to obtain a comprehensive picture of these processes.

The synergy between experimentally determined results and theoretical models continues to be one of the most important interactions in science. This relationship in the field of detonation science shares a common significance. Numerous research endeavors are being pursued to develop full equations of state for materials, which depend

on the quality of theoretical models. The accuracy of current models and hydrocodes depends on the accuracy of parameters evaluated and validated from experiments. The body of experimental data that comprises dynamical thermal properties of materials in extreme conditions is narrow and needs to be expanded to advance our understanding of heat transfer in shock conditions.

The fluorescence from ruby crystals is known to exhibit a strong pressure and temperature dependence.[1,2] The ruby crystal has become a common pressure transducer in current, static high-pressure research in diamond anvil cells and has displayed a response time as short as 30 ns.[3-5] The fast pressure and temperature responses make ruby an ideal probe of transient mechanical and thermal events.

This paper will expand upon two recent publications in which sodium chloride (NaCl) was used as the material of interest.[6,7] A pressure-dependent set of data was presented that demonstrates the efficacy of such a technique for extracting thermal transport properties, which are difficult to attain. These parameters include thermal conductivity (k), thermal diffusivity ($\alpha$) and heat capacity ($C_p$). Experimental efforts for NaCl and Teflon will be discussed. Also, a more detailed description of the mathematical solution to the heat conduction equation will be presented with an application towards extracting thermal properties from experimental data.

## EXPERIMENTAL METHOD

A Merrill-Basset anvil cell[8] with single-crystal cubic zirconia (CZ) anvils was used in each experiment. A close-up view of the anvil configuration is shown in Fig. 1. The entire cell was encased in stainless steel (not shown) and the opposing CZ anvils were used to compress a desired material to pressures in the 0.05 GPa to 3.0 GPa range. Inconel gaskets (250 μm thick and a 300 μm diameter hole) were used to confine the pressurized test material. A 3 μm thick aluminum foil separated equal halves of the sample (NaCl or Teflon) and was used as target for laser heating.

A ruby sphere (30-40 μm diameter) was embedded in the material under study (shown as a small circle to the right of the Aluminum foil in Fig. 1). A Cynosure pulsed dye laser (labeled "L1" in Fig. 1) was used to initiate a thermal wave in the sample cell by quickly heating the Aluminum foil (heating pulse is 4 μs long at 514 nm; and incident on the foil on the opposite side as the ruby). This heating pulse defined the time (t) of the experiment, where t=0. Incident laser fluences from 2 to 5 J-cm$^{-2}$ were typical. The aluminum foil absorbed approximately 15% of the incident energy due to reflective losses at surfaces.

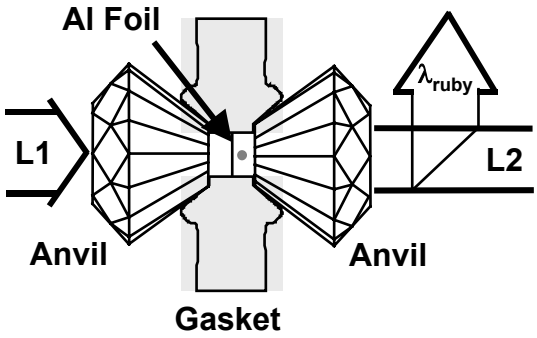


**FIGURE 1. VIEW OF THE EXPERIMENTAL ANVIL CELL.**

Time-resolved diffusion of heat through the selected material was monitored through changes in the peak positions of the $R_1$ fluorescence line of the ruby sphere. The ruby was placed a known distance from the aluminum target (25-50 μm measured *in situ* by a high-resolution optical microscope). Ruby fluorescence followed the absorption of 532 nm light from a Spectra Physics solid-state laser (labeled "L2" in Fig. 1). The fluorescence (near 690 nm, labeled "$\lambda_{ruby}$" in Fig. 1) was collected back along the same pathway as the incident 532 nm light, split with a dichroic optic and dispersed in a monochromator (Holospec f1.8i, Kaiser) according to wavelength. Time-resolution was achieved in a light dispersing streak camera (Hamamatsu 2830) orthogonal to the spectral dispersion. Spectra were recorded on a CCD camera as a 2-Dimensional set of data with wavelength and time dependence.

## SOLUTIONS TO THE HEAT CONDUCTION EQUATION

Two sets of solutions to the heat conduction equation (Eq. 1) were used to help analyze the experimental data. They will be referred to as the Inverse and Direct models. The heat conduction equation is used to describe the propagation of heat in a solid material.

$$\nabla \cdot \left(k(T,P)\nabla T\right) = \rho C_p(T,P)\frac{\partial T}{\partial t} \qquad (1)$$

k denotes the material's thermal conductivity, $C_p$ its heat capacity and ρ its density. By Fourier's Law, thermal conductivity is the proportionality constant between the temperature gradient ($\nabla T$) within the material and the heat flux ($\varphi$).

$$\varphi = -k(T,P)\nabla T \qquad (2)$$

Since the anvil is composed of several different materials arranged in a complex geometry, all of these parameters may vary with position. Moreover, the irregular geometry precludes the application of standard analytical techniques such as separation of variables. The irregular geometry and composite nature of the anvil cell is readily handled by a numerical method such as finite element analysis.

### Inverse (Analytical) Model

A 1-dimensional (1-D) analytical model of the heat flow in a material was derived to extract the desired thermal transport properties from the measured thermal wave. The heat flow in Fig. 1 can be considered a one-dimensional spatial problem at early times before heat transfer to the surrounding gasket is discernible, and by noting that the ruby diameter is much smaller than the foil width. In this model, it is assumed that the heat pulse of the laser is much faster than the thermal relaxation time scale within the solid.

This model utilizes the axial symmetry of the experimental anvil cell and assumes a continuous heat flux at the interface between different materials in the cell (no interfacial contact resistance). The flow of heat in one dimension can be described by the following partial differential equation (PDE):

$$\frac{\partial}{\partial z}\left(k\frac{\partial \theta}{\partial z}\right) = \rho C_p \frac{\partial \theta}{\partial t} \qquad 0 < z < L$$

$$\theta(z,t) \equiv T(z,t) - T_0 \equiv \Delta T \qquad (3)$$

where "z" denotes the axial coordinate and $T_0$ is the initial temperature. As a first approximation, radial flow of heat in the material is ignored ("r"; refer to Fig. 2 for a diagram of the dimensions).

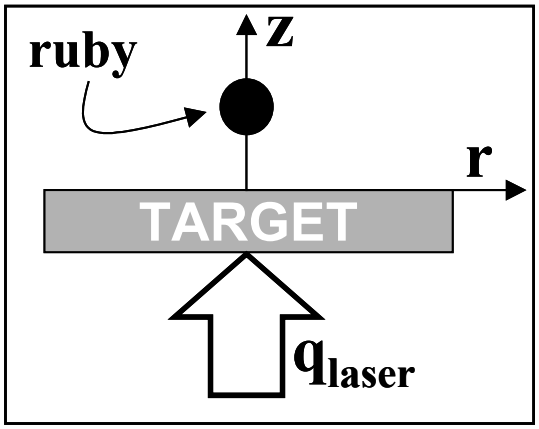


**FIGURE 2: CARTOON REPRESENTING 1-D ANALYTICAL MODEL OF HEAT FLOW.**

The Laplace transform of Eq. (3) yields an ordinary differential equation in s-space for the transformed temperature ($\hat{\theta}$):

$$\frac{d}{dz}\left(\frac{d\hat{\theta}}{dz}\right) = \frac{\rho C_p s\hat{\theta}}{k} = \frac{s\hat{\theta}}{\alpha} \qquad (4)$$

assuming k is constant within the z domain. The assumption that thermal parameters are independent of temperature is reasonable for this experiment as temperature changes are very small

and confined to a small region near the aluminum target. α is the thermal diffusivity, which is also treated as a temperature-independent parameter. The general solution to Eq. 4 is given by:

$$\theta = A(s)e^{\left(-\sqrt{\frac{s}{a}}\cdot z\right)} + B(s)e^{\left(+\sqrt{\frac{s}{a}}\cdot z\right)} \qquad (5)$$

The integration constants A(s) and B(s) are determined by the boundary conditions at z=0 and z=L. For sufficiently short time, the boundary at z=L can be considered to be at infinity (z→∞) and the second term would diverge. Thus, an approximate solution can be constructed by setting B(s)=0. The effects of a finite boundary (z=L) can be readily incorporated at the expense of algebraic complexity. The boundary condition at z=0 determines A(s):

$$-k\frac{d\theta}{dz} = k\sqrt{\frac{s}{\alpha}}\cdot A(s) = q(s) \qquad (6)$$

where "q(s)" is the transformed (t→s) laser flux (W/cm$^2$). The solution for $\hat{\theta}$(z,s) is given by:

$$\hat{\theta} = \frac{q(s)}{k}\cdot\sqrt{\frac{\alpha}{s}}\cdot e^{\left(-\sqrt{\frac{s}{\alpha}}\cdot z\right)} = \Delta\hat{T} \qquad (7)$$

Taking the inverse transform (s→t) of Eq. 7 gives the time-domain solution for ΔT(z,t):

$$\Delta T(z,t) = \frac{q}{2k}\cdot\sqrt{\frac{\alpha}{\pi\cdot t}}\cdot e^{\left(\frac{-z^2}{4\cdot\alpha\cdot t}\right)} \qquad (8)$$

The inversion assumes that q(t) is a delta function in t. The experimentally measured temperature profiles were fit to Eq. (8) using a two-parameter (k, α) regression analysis. The factor of two in the denominator of Eq. 8 was included because heat flow was only being measured by experiments in the "+z" dimension (equal heat flows towards "-z"). The heat capacity ($C_p$) can be easily determined with a knowledge of the density of the solid according to the relation:

$$C_p = k/\rho\alpha \qquad (9)$$

**Direct Model**

FlexPDE software (Version 3, PDE Solutions Inc.) was used to solve the heat conduction equation (Eq. 1) in our second model. This software package utilizes a finite-element technique to solve 3-dimensional time-dependent partial differential equations. The equations may be nonlinear and coupled.

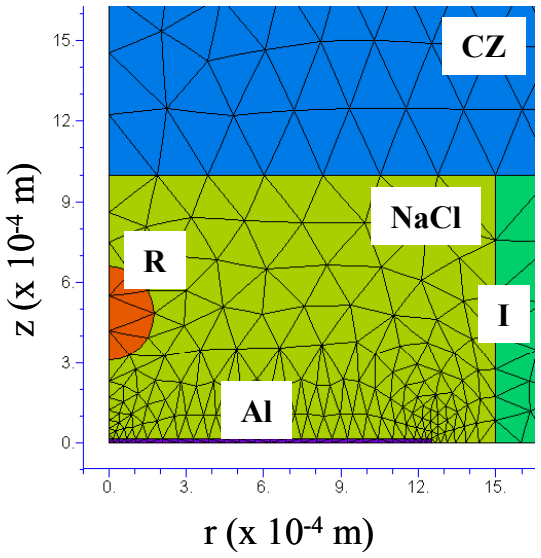


**FIGURE 3: VIEW OF INPUT STRUCTURE FOR FLEXPDE SIMULATIONS. SEE TEXT FOR MATERIAL ABREVIATIONS.**

A text input file describing the physical boundary conditions, model equations, and variables provides the backbone for each calculation. The temperature dependence of thermal properties in the materials can be used, creating a complex set of non-linear differential equations for the temperature within the anvil. A personal computer can be used to solve these equations for any desired time step with reasonable computer time.

FlexPDE sets up a triangular grid from which numerical results are tabulated. The grid density automatically adjusts to meet the user-defined error in the calculations. A typical grid is shown above (Fig. 3), exhibiting the higher grid density near the aluminum foil where the temperature gradient and numerical difficulty is heightened.

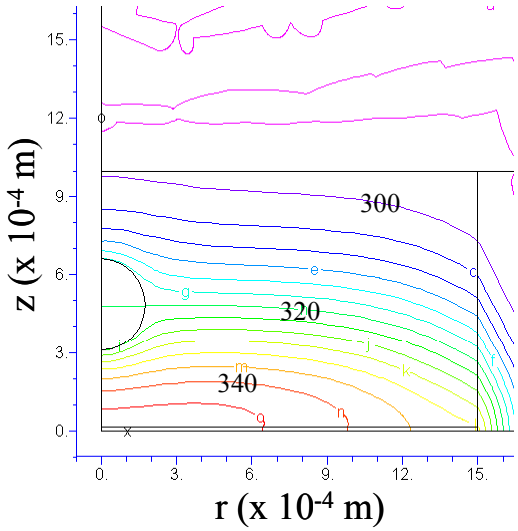


**FIGURE 4: SNAPSHOT OF ISOTHERMS IN NACL CALCULATED BY FLEXPDE 300 μS AFTER THERMAL WAVE INITIATION.**

Each material is inserted into the cylindrically symmetric coordinate system with its respective thermal properties. The materials in Fig. 3 are abbreviated as follows: cubic zirconium anvils (CZ), sodium chloride (NaCl), Inconel gaskets (I), ruby (R), and aluminum foil (Al). The view offered in Fig. 3 and some of the following figures is a reduced (zoomed) portion of the entire physical space (150 μm x 150 μm). Great care was taken to reproduce the boundaries and dimensions of the experimental set-up.

Figure 4 is a snapshot of the isotherms calculated for NaCl 300 μs after the initiation of a thermal wave. This displays the ability of FlexPDE to thoroughly describe the thermal gradients at each time step. It also demonstrates the quasi-one-dimensional nature of the heat flow and supports the assumptions made in the inverse model described previously.

A thermal stress model was developed and incorporated into FlexPDE to determine the possible contribution of a pressure wave to the measured temperatures.[7] The stress response falls into two distinct time domains. The short time domain corresponds to a pressure wave traveling at the speed of sound ($4.7 \times 10^5$ cm/s). The pressure wave (or sound wave) was determined to traverse the medium on a much quicker time scale (0.3 ns) than the thermal wave that follows so it should not contribute to the ruby fluorescence line shifts on our experimental time scale.

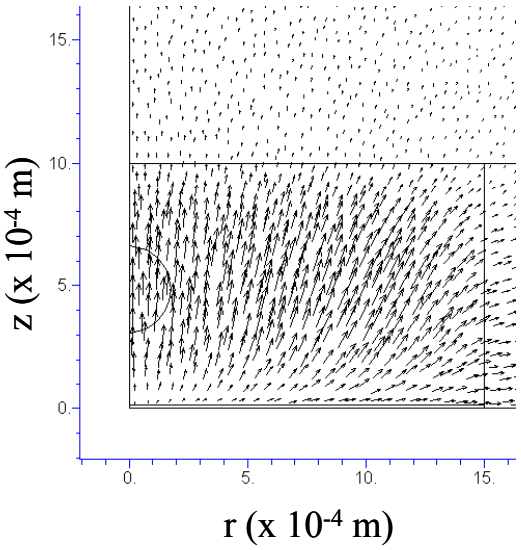


**FIGURE 5: SNAPSHOT OF DISPLACEMENT VECTORS CALCULATED BY FLEXPDE 300 μS AFTER THERMAL WAVE INITIATION.**

There is a long-time component of stress associated with the variable thermal expansion properties of the materials within the cell. It was concluded that this quasi-static component should be less than the experimental noise (< 2 Kbar). Fig. 5 shows the associated physical displacement of material that accompanies the quasi-static thermal wave on our experimental time scale (300 μs is chosen). In this figure, the magnitude of the vectors was scaled up by a factor of $10^4$.

FlexPDE has the ability to analyze the diffusion of heat and the mechanical properties of a selected material at any desired time interval. This is a powerful tool for analyzing experimental results and verifying the validity of analytical models developed to determine physical properties at high pressures. It is also a valuable predictive tool for future experiments.

## RESULTS AND DISCUSSION

A typical set of fluorescence data is presented in Fig. 6, following the initiation of a thermal wave in sodium chloride. Spectra were recorded at 40 μs intervals and the specific times of each spectrum are labeled in Fig. 6. The peak positions of each spectrum (highlighting the $R_1$ spectral feature with a line in this case) were deduced from a fit to a lorentzian line shape. The peak positions were reduced to absolute temperatures following the $R_1$ temperature dependence of 0.068 Å/K.[1,2]

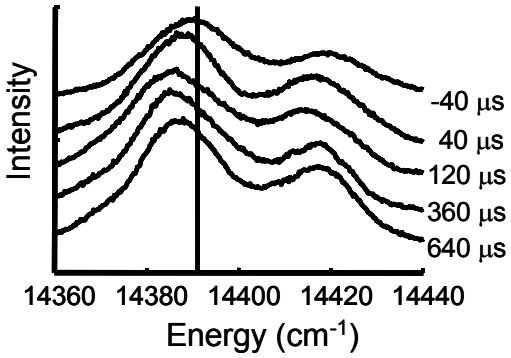


**FIGURE 6: TIME-RESOLVED RUBY FLUORESCENCE SPECTRA EXHIBITING THE PROGRESSION OF A THERMAL WAVE VIA ENERGY SHIFTS IN ITS EMISSION LINES.**

Once the data was converted to temperature, it could be plotted vs. time similar to Fig. 7. The data presented in this figure is reproduced from a previous publication where the pressure of the NaCl sample is held constant at 0.05 GPa and the laser flux is 4.94 J-cm$^{-2}$.[7] The data can be fit by a regression analysis with Eq. 8, solving for k and α. The fit is shown as a solid line in Fig. 7. k was determined to be 5.0 W-m$^{-1}$K$^{-1}$ and α was 2.84 x 10$^{-6}$ m$^2$-s$^{-1}$. $C_p$ must be 47.5 J-mol$^{-1}$K$^{-1}$ following the relationship in equation 9 at a density (ρ) of 2.16 x 10$^6$ g-m$^{-3}$.

The entire set of NaCl data at varying laser fluences and pressures was determined in the same fashion and tabulated in Ref. 7. The major trends observed include increasing thermal properties with increasing pressure (k, α, $C_p$) and decreasing laser power (k, α). A more quantitative analysis of these trends is currently being pursued.

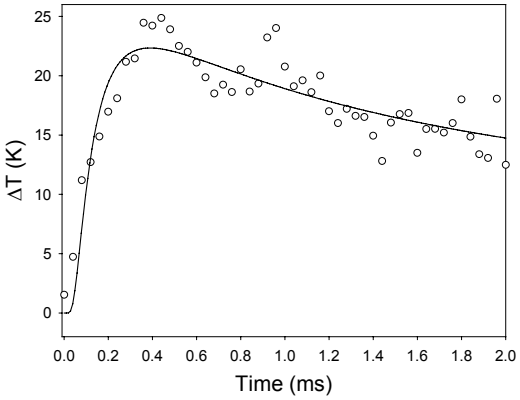


**FIGURE 7: 1-D ANALYTICAL FIT (LINE) TO THERMAL WAVE DATA (CIRCLES) FOR NACL AT 0.05 GPA.**

Initial experiments using Teflon as a test material did not generate an analogous set of results. Ruby fluorescence lines did not indicate a substantial temperature rise in Teflon out to 1 ms. FlexPDE was a valuable tool for analyzing this experimental hurdle. Fig. 8 is a comparative plot for the thermal waves measured in NaCl and Teflon. The thermal wave of NaCl (solid line) reaches a temperature maximum prior to 1 ms. However, the simulated temperature maximum for Teflon extends out near 4 ms and the overall profile is much broader. This can be ascribed to the expected difference in thermal conductivities (a factor of 10 less for Teflon).

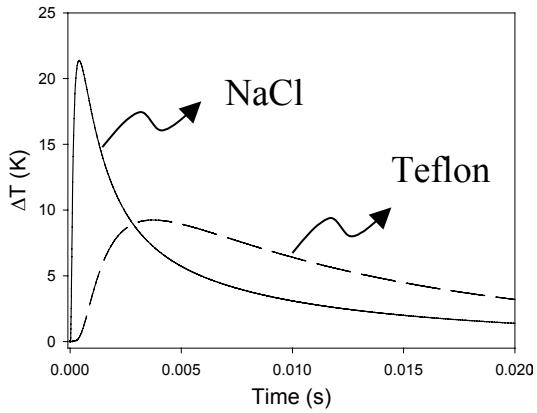


**FIGURE 8: SIMULATIONS OF THE PROGRESSION OF A THERMAL WAVE IN NACL (SOLID) AND TEFLON (DASHED).**

It is obvious from these results that the time frame for data acquisition must be extended to meet the slower temporal response of Teflon. A less sensitive temperature response is also expected if the ruby is placed near the same position as it was in the NaCl experiments. The thermal parameters used in this simulation were from ambient test conditions.[9]

## CONCLUSIONS

The spectroscopic method outlined in this proceeding is effective in determining the thermal properties of materials at elevated pressures. The 1-D analytical model permits the extraction of these valuable parameters from experimental data and FlexPDE provides a dynamic picture of the thermal wave, which will be used in future analysis as a quantitative tool.

Sodium chloride results match well to previously determined values. Teflon measurements are ongoing and FlexPDE simulations have provided a "ballpark" timescale with which to work.

Future experiments will set out to measure thermal properties of energetic materials at even higher pressures and through phase changes. A quantitative study of the temperature dependence of thermal properties will also be examined from a combination of fluence-dependent studies and FlexPDE simulations.

## ACKNOWLEDGMENTS

We would like to acknowledge the Naval Surface Warfare Center at Indian Head (ILIR program) for funding of this project.

## REFERENCES

1. Barnett, J. D., Block, S., and Piermarini, G. J., Rev. Sci. Instrum. **44**, 1 (1973).
2. Piermarini, G. J. and Block, S., Rev. Sci. Instrum. **46**, 973 (1975).
3. Horn, P. D. and Gupta, Y. M., Phys. Rev. B **39**, 973 (1989).
4. Sharma, S. M. and Gupta, Y. M., Phys. Rev. B **43**, 879 (1991).
5. Gupta, Y. M. and Shen, X. A., Appl. Phys. Lett. **58**, 583 (1991).
6. Pangilinan, G. I., Ladouceur, H. D. and Russell, T. P., Appl. Phys. Lett. **76** 2460 (2000).
7. Pangilinan, G. I., Ladouceur, H. D. and Russell, T. P., Rev. Sci. Instrum. **71**, 3846 (2000).
8. Merrill, L. and Bassett, W. A., Rev. Sci. Instrum. **45**, 290 (1974).
9. *Thermophysical Properties of Matter*, edited by Toulokian, Y. S., Powell, R. W., Ho, C. Y. and Klemens, P. G. (Plenum, New York, 1970).